

DeepPerception: Advancing R1-like Cognitive Visual Perception in MLLMs for Knowledge-Intensive Visual Grounding

Xinyu Ma¹, Ziyang Ding⁴, Zhicong Luo³, Chi Chen^{2, †}, Zonghao Guo²,
Derek F. Wong^{1, †}, Xiaoyi Feng³, Maosong Sun²

¹University of Macau, ²Tsinghua University,
³Northwestern Polytechnical University, ⁴Shandong University

chenchithu@gmail.com, derekfw@um.edu.mo

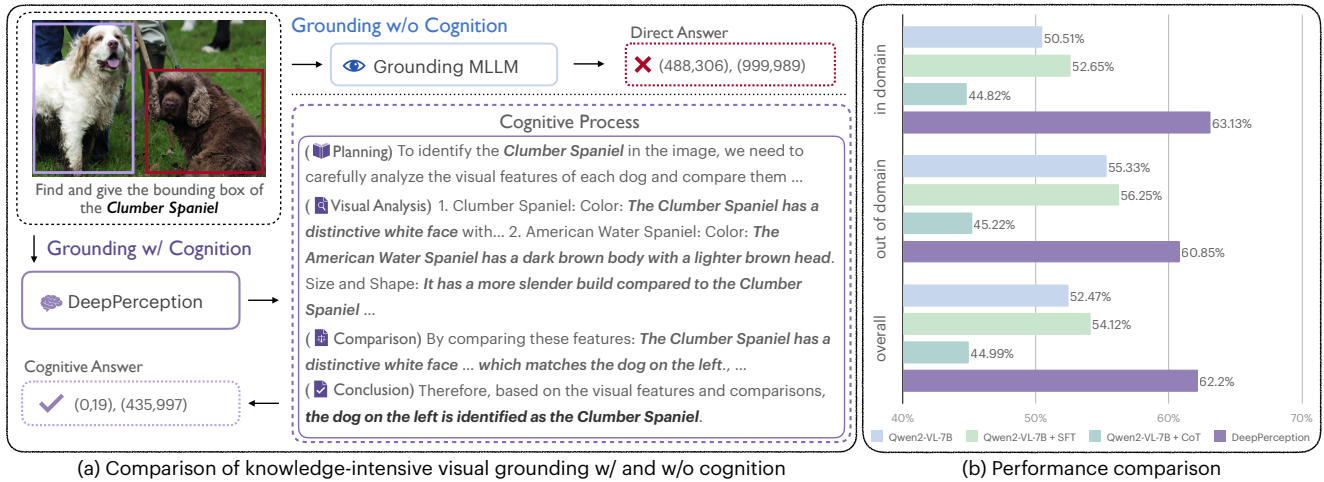


Figure 1. (a) DeepPerception employs knowledge-driven reasoning to derive answers, while the baseline model directly outputs predictions without cognitive processing. (b) DeepPerception demonstrates superior cognitive visual perception capabilities that cannot be elicited in the foundation model through simplistic zero-shot CoT prompting.

Abstract

Human experts excel at fine-grained visual discrimination by leveraging domain knowledge to refine perceptual features, a capability that remains underdeveloped in current Multimodal Large Language Models (MLLMs). Despite possessing vast expert-level knowledge, MLLMs struggle to integrate reasoning into visual perception, often generating direct responses without deeper analysis. To bridge this gap, we introduce knowledge-intensive visual grounding (KVG), a novel visual grounding task that requires both fine-grained perception and domain-specific knowledge integration. To address the challenges of KVG, we propose DeepPerception, an MLLM enhanced with cognitive visual perception capabilities. Our approach consists of (1) an automated data synthesis pipeline that generates high-quality, knowledge-aligned training samples, and (2) a two-stage training framework combining supervised fine-tuning for cognitive reasoning scaffolding and reinforcement learning

to optimize perception-cognition synergy. To benchmark performance, we introduce KVG-Bench, a comprehensive dataset spanning 10 domains with 1.3K manually curated test cases. Experimental results demonstrate that DeepPerception significantly outperforms direct fine-tuning, achieving +8.08% accuracy improvements on KVG-Bench and exhibiting +4.60% superior cross-domain generalization over baseline approaches. Our findings highlight the importance of integrating cognitive processes into MLLMs for human-like visual perception and open new directions for multimodal reasoning research. The data, codes, and models are released at <https://github.com/thunlp/DeepPerception>.

[†]Corresponding authors

1. Introduction

Human experts demonstrate enhanced fine-grained discrimination of visual concepts by flexibly leveraging domain knowledge to refine discriminative features, resulting in superior domain-specific visual perception compared to non-experts [9, 12, 33]. However, despite their possession of expert-level knowledge [47], current Multimodal Large Language Models (MLLMs) struggle to effectively utilize this knowledge for visual perception in the same way human experts do. This is primarily because current MLLMs often directly generate final answers to questions without deeper analysis [41, 43]. Consequently, when questions require knowledge and analytical reasoning, this direct-response mode frequently results in errors as illustrated in Fig. 1a.

In this paper, we explore how to enhance MLLMs with **cognitive visual perception** capabilities, i.e., to integrate the inherent knowledge and reasoning capacities of MLLMs into the processing of visual perception tasks. Accordingly, we propose *knowledge-intensive visual grounding* (KVG), a novel visual grounding task [13, 46] that advances conventional visual grounding by requiring both fine-grained visual perception and domain-specific knowledge integration. As shown in Fig. 1a, each query in KVG utilizes domain-specific terminology (“Clumber Spaniel”) rather than generic descriptions (“the left dog”). Moreover, the images contain distracting objects that require knowledge-based reasoning to differentiate and answer correctly. Unlike the mathematical and geometric tasks studied by previous multimodal reasoning LLMs [41, 43], KVG focuses more on the role of cognition in fundamental visual perception processes.

To solve the KVG task, an MLLM must first engage in a cognitive process, leveraging relevant domain knowledge, and conduct a thorough visual analysis before providing a final perceptual response. However, we find this task challenging for current MLLMs. For instance, the accuracy of Qwen2-VL-7B [36] on this task is only around 50% (Fig. 1b), while on traditional visual grounding dataset RefCOCO [46], it exceeds 90% [36]. Furthermore, when explicitly prompting the model to perform the cognitive process, the results drop significantly, which indicates that current MLLMs do not possess this capability.

In order to advance MLLMs with cognitive visual perception, we introduce a cognition-enhanced training framework comprising: (1) an automated data synthesis pipeline that alleviates the scarcity of high-quality training data by synthesizing knowledge-aligned samples from fine-grained visual categorization datasets, and (2) a two-stage training framework where supervised fine-tuning establishes foundational cognitive capabilities through knowledge-integrated reasoning chains, followed by reinforcement learning that optimizes perception-cognition synergy via

perception-oriented reward signals. This integrated approach ensures systematic progression from perception-oriented reasoning to precision-driven perceptual refinement while maintaining training stability, effectively bridging the gap between MLLMs’ inherent cognition capability and human-like visual perception. Through this framework, we develop **DeepPerception**, an MLLM that enhances visual perception through inherent cognition capability.

To facilitate systematic evaluation on KVG, we introduce KVG-Bench, a comprehensive benchmark encompassing 10 distinct domains with 1.3K manually curated test cases linked to 531 images and 882 entities. Our extensive experiments across KVG and related tasks reveal two key findings: (1) Our DeepPerception model achieves substantial performance gains over direct fine-tuning (average +8.08% accuracy), demonstrating its effectiveness in activating models’ cognitive visual perception capabilities; (2) Notably, DeepPerception exhibits superior cross-domain generalization on unseen domains compared to existing approaches (e.g., +4.60% over fine-tuning), demonstrating its ability to enhance visual perception through intrinsic cognitive mechanisms rather than mere entity memorization.

In summary, our contributions are threefold:

- We introduce the task of knowledge-intensive visual grounding (KVG) to explore the concept of cognitive visual perception for MLLMs, aiming to integrate their inherent knowledge and reasoning capabilities into visual perception.
- We propose DeepPerception, an MLLM with enhanced cognitive visual perception capabilities. To achieve this, we develop an automated dataset creation pipeline and a two-stage framework integrating supervised cognitive capability enhancement with perception-oriented reinforcement learning.
- We introduce KVG-Bench, a manually curated benchmark for the KVG task involving diverse knowledge domains and entities. Experiments on KVG-Bench and other fine-grained visual recognition tasks demonstrate DeepPerception’s exceptional cognitive visual perception capabilities and superior cross-domain generalization performance.

2. Related Work

2.1. Multimodal Large Language Models

Recent years have witnessed rapid advancements in MLLMs [6, 19, 20, 28, 36, 44], with visual grounding [3, 17, 23, 29, 45] and reasoning [8, 32, 41, 48] emerging as their pivotal capabilities. For visual grounding, Shikra [3] introduces a streamlined end-to-end architecture that allows the model to process spatial input and generate the corresponding visual references. Groma [23]

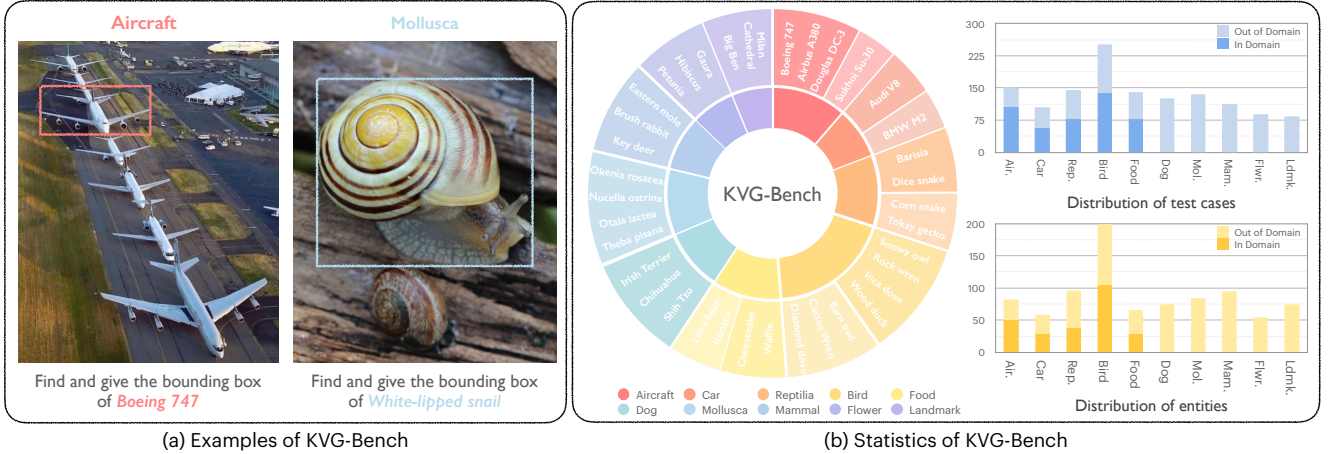


Figure 2. (a) KVG-Bench images contain multiple subordinate-category entities (e.g., Boeing 777, 767, 757, 747, 737, 727, 717, 707 from top to bottom in the left image); (b) KVG-Bench exhibits high diversity across categories and entities.

partitions images into multiple regions during tokenization, thereby improving the grasp of the visual information of the model. Regarding reasoning capabilities, MathLLaVA [32] and LLaVA-CoT [41] advances multimodal reasoning through fine-tuning on their synthesized datasets. Notably, LISA [17] uniquely bridges these capabilities by applying MLLM reasoning to visual grounding tasks. In contrast, our work aims to further empower models with expert-level reasoning capabilities to achieve cognitive visual perception.

2.2. Fine-grained Visual Perception Benchmarks

Visual Grounding aims to locate objects or regions within an image based on a textual query [13, 30, 46]. To enable a more comprehensive evaluation of MLLMs’ visual grounding capabilities, researchers have recently proposed numerous novel and more challenging benchmarks [4, 5, 17, 21] in addition to the most widely adopted RefCOCO/+g benchmarks [13, 25]. SK-VG [5] focuses on visual grounding with scene knowledge integration as additional input, whereas ReasonSeg [17] requires world knowledge utilization for object localization. Fine-Grained Visual Recognition (FGVR) aims to classify visually similar images to subcategories with a super-category [14, 16, 24, 26, 38]. Our proposed KVG task synergistically combines visual grounding and FGVR, simultaneously demanding expert-level knowledge for distinguishing subordinate categories and precise grounding capabilities.

3. KVG-Bench

3.1. Task Definition

The task of knowledge-intensive visual grounding (KVG) is to predict a bounding box $B = f_{\theta}(X_I, X_T)$ through joint understanding of visual input X_I and textual query X_T ,

requiring fine-grained alignment between multimodal representations. While sharing structural similarities with referring expression comprehension (REC), this task significantly elevates the challenge beyond standard REC tasks. As exemplified in Fig. 2a, the queries of KVG involve fine-grained entity specifications (e.g., “Boeing 747”) rather than generic categories such as “aircraft”. Additionally, each image contains multiple objects from the same category of the target object (e.g., multiple aircraft in a single image). This setup requires both expert-level knowledge and advanced perceptual and reasoning abilities to pinpoint the precise features that distinguish the target from similar objects.

3.2. Benchmark Construction

KVG-Bench comprises 1,336 test instances spanning 10 categories with 882 distinct entities, as statistically visualized in Fig. 2b. The construction includes two key parts: image collection and data annotation.

We designed a meticulous collection process to ensure the diversity and complexity of the images. First, we carefully selected 10 categories from the field of fine-grained visual recognition (FGVR) [14, 16, 24, 26, 38] that are suitable for visual grounding, excluding categories which are challenging for object localization such as “sports” and “scene”. Second, an entity list for each category was systematically developed through initial extraction of fine-grained labels from existing datasets, followed by comprehensive enrichment of entity names via ChatGPT-assisted expansion. We then retrieved web images using these entity names as search queries, enforcing strict quality criteria: each image must contain at least two entities from the same category with clear visual disparities.

The annotation process prioritized quality control. Five annotators manually annotated each image with bounding

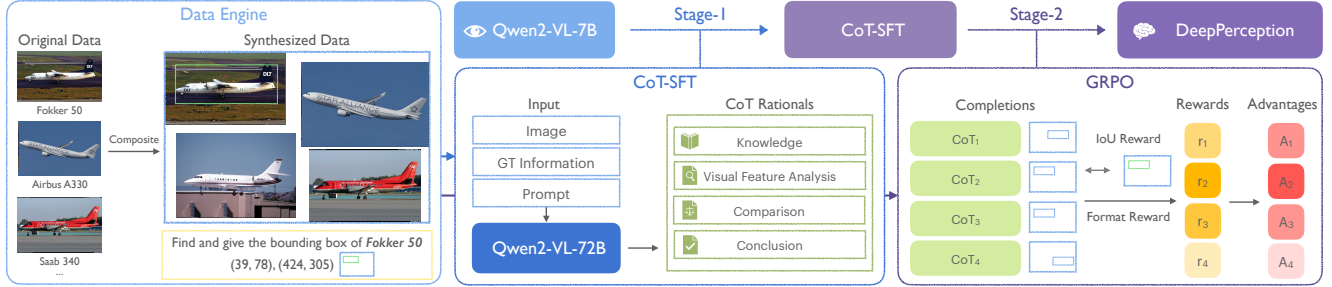


Figure 3. Overview of the proposed data engine and two-stage training framework.

boxes and entity labels by cross-referencing contextual information (e.g. caption, webpage metadata) with authoritative sources (e.g., Wikipedia entries) to verify entity identities. To ensure consistency, the annotations underwent independent re-evaluation by annotators who did not participate in the initial labeling, with conflicting cases cross-verified through multi-annotator reconciliation and persistently inconsistent instances eliminated to ensure annotation accuracy. By integrating strict validation protocols and expert-aligned annotation workflows, KVG-Bench sets a new standard for evaluating cognitive visual perception in multimodal systems.

3.3. Human Evaluation

To assess the difficulty of KVG-Bench, we conducted human evaluations with 11 non-expert volunteers under two experimental settings: Closed-Book (no external resources) and Open-Book (single Wikipedia query/case to simulate expert-level knowledge integration). Participants were randomly assigned several categories, with each category at least five evaluators to mitigate knowledge bias. The evaluation results, as shown in Tab. 1, reveal significant performance differences between settings. The Open-Book Setting demonstrated significant performance elevation (78.83% accuracy) compared to Closed-Book results (56.41%). This validates that KVG-Bench requires synergistic integration of expert-level knowledge and fine-grained visual comparison, positioning it as a meaningful testbed for advancing cognitive visual perception in MLLMs.

4. Method

While current MLLMs demonstrate inherent grounding capabilities, as demonstrated in Fig. 1, their direct answer paradigm lacks reasoning mechanisms to synergize cognitive processing with visual perception, resulting in suboptimal performance for the KVG task. The absence of explicit reasoning pathways prevents effective integration of domain knowledge with visual understanding, particularly in scenarios requiring multi-step cognitive operations. Draw-

ing inspiration from the remarkable success of DeepSeek-R1 [10], we proposed a two-stage training framework (See Fig. 3), which enables systematic development of cognitive visual perception capability while maintaining training stability.

4.1. Data Engine

The training data images for KVG must meet the following criteria: (1) they should include expert-level entity and bounding box annotations, and (2) the images should contain multiple similar objects to ensure the difficulty of the task. To overcome the scarcity of such data, we developed an automated pipeline leveraging FGVR datasets as the data source. First, data from multiple FGVR datasets were categorized into ten categories (as shown in Fig. 2). The first five categories were used directly for training, while the last five were used solely as unseen categories, with their data not being used for training. Since there are no bounding box annotations in the original FGVR datasets, we employed Qwen2VL-7B [36] to generate bounding boxes through entity-specific prompts (e.g., “Find and give the bounding box of Airbus A330”). With entity labels pre-verified for presence, this automated method achieved over 95% accuracy, validated through manual checks. To overcome the limitation of single-object dominance in existing datasets, as illustrated in Fig. 3, we synthesized composite images containing at least 2 entities from the same category (e.g., multiple dog species in one image) using horizontal, vertical, grid, or random layouts, adjusting bounding box coordinates to preserve annotation consistency while enforcing entity uniqueness. This approach requires models to perform fine-grained visual comparisons through structured cognitive processes rather than relying on memorization. The final dataset, partitioned for two-stage training, balances real-world complexity with quality control, simulating scenarios demanding cognitive visual perception.

4.2. Chain-of-Thought Supervised Fine-Tuning

The primary objective of the first stage training is to endow models with visual perception-oriented cognitive capabilities through synthesized CoT training data. This pro-

cess fosters an initial cognitive-perceptual synergy by explicitly modeling reasoning trajectories in the KVG task while establishing fundamental knowledge association patterns for subsequent optimization. Specifically, we leveraged the powerful Qwen2-VL-72B [36] model to generate CoT reasoning data. As illustrated in Fig. 3, we generated CoT rationales by inputting images, ground-truth annotations (labels and bounding boxes), and CoT reasoning prompts into the model. This process synthesizes reasoning chains that combine the model’s domain knowledge with human-like cognitive processes (e.g., iterative hypothesis verification through joint domain knowledge and visual feature analysis). We then performed SFT on the Qwen2-VL-7B model using these data, yielding the stage-1 model with foundational cognitive visual perception capabilities. This model demonstrates preliminary abilities to integrate domain knowledge and generate stepwise reasoning chains for visual grounding, which serves as a stable foundation for the second-stage reinforcement learning training. This approach bridges the gap between raw perception and expert-level cognition, enabling models to emulate human-like visual perception through knowledge-visual co-verification.

4.3. Perception-oriented Reinforcement Learning

Following the initial CoT-SFT training, we conducted reinforcement learning using a separate subset of training data to further enhance the model’s perception capabilities, building upon its acquired cognitive visual perception foundation. As illustrated in Fig. 3, we adopted GRPO following Guo et al. [10], which optimizes the policy model by sampling a group of outputs to a question and calculating a group-relative advantage instead of a critic model. To adapt GRPO for visual grounding tasks, we designed a rule-based reward system and performed data filtering on the training data using the stage-1 model.

Training Objective. Let q denote the question and $\{o_1, \dots, o_G\}$ denote the sampled outputs from the old policy model $\pi_{\theta_{old}}$, then the optimization objective of policy model π_{θ} can be formally defined as:

$$\mathcal{J}_{GRPO}(\theta) = \mathbb{E} \left[q \sim P(Q), \{o_i\}_{i=1}^G \sim \pi_{\theta_{old}}(O | q) \right] \frac{1}{G} \sum_{i=1}^G \left(\frac{\pi_{\theta}(o_i | q)}{\pi_{\theta_{old}}(o_i | q)} A_i - \beta \mathbb{D}_{KL}(\pi_{\theta} || \pi_{ref}) \right) \quad (1)$$

$$\mathbb{D}_{KL}(\pi_{\theta} || \pi_{ref}) = \frac{\pi_{ref}(o_i | q)}{\pi_{\theta}(o_i | q)} - \log \frac{\pi_{ref}(o_i | q)}{\pi_{\theta}(o_i | q)} - 1 \quad (2)$$

where ε and β are hyper-parameters and A_i is the advantage computed based on a group of rewards $\{r_1, \dots, r_G\}$ corresponding to the outputs of each group:

$$A_i = \frac{r_i - \text{mean}(\{r_1, \dots, r_G\})}{\text{std}(\{r_1, \dots, r_G\})} \quad (3)$$

Reward Modeling. We adopted a rule-based reward system specifically tailored for visual grounding tasks, comprising two types of rewards: Intersection over Union (IoU) reward and Format reward. The IoU reward evaluates the spatial alignment between predicted bounding boxes and ground-truth annotations. Given the ground-truth bounding box B and the predicted bounding box \tilde{B} , the IoU reward is formally defined as:

$$R_{IoU} = \begin{cases} \text{IoU}(B, \tilde{B}), & \text{if } \text{IoU}(B, \tilde{B}) \geq \tau \\ 0, & \text{otherwise} \end{cases} \quad (4)$$

where τ denotes the alignment threshold for valid spatial grounding. In contrast to the conventional binary accuracy reward (0/1) based solely on final answer correctness, our continuous IoU reward delivers finer-grained supervision signals proportional to spatial prediction quality. By introducing an alignment threshold τ , this design effectively prevents reward hacking through degenerate bounding boxes (e.g. [0, 0, 1000, 1000]) that exploit low-IoU predictions. The format reward employs regular expression-based pattern matching to enforce strict structural separation between reasoning processes and final answers, ensuring cognitive rationales are encapsulated within ‘;think_i’ and ‘;think_i’ tags while grounded predictions reside within ‘;answer_i’ and ‘;answer_i’. In addition, we imposed constraints on the bounding box format to ensure correct output structure.

Data Filtering. To enhance training efficiency, we implemented a strategic data filtering using the stage-1 CoT-SFT model. Specifically, we performed multiple sampling passes on the training data and filtered out cases where all samples were either fully correct (deemed too trivial for further training) or entirely incorrect (considered too challenging for performance improvement through repeated sampling). This approach ensures the model focuses on learnable instances where partial correctness provides actionable optimization signals, thereby maximizing training effectiveness while mitigating exposure to uninformative extremes.

5. Experiment

5.1. Implementation Details

Datasets. We conducted experiments based on several FGVR datasets including FGVC-Aircraft [24], Stanford-Cars [16], iNaturalist2017 [35], Food101 [2], Stanford-Dogs [14], Flower-102 [26], and Google-Landmarks-v2 [39]. Notably, as detailed in Sec. 4.1, only a subset of the aforementioned datasets was utilized for KVG training, with 25K samples for stage-1 followed by 4K filtered instances for stage-2 training.

Baseline Models. We built DeepPerception upon Qwen2-VL-7B [36] for its top visual grounding capability and

¹reproduced using VLMEvalKit

Models	Seen Categories						Unseen categories						Avg.
	Air.	Car	Rep.	Bird	Food	Avg.	Dog	Mol.	Mam.	Flwr.	Ldmk.	Avg.	
Human Evaluation													
Human	59.33	66.67	50.84	44.17	65.33	57.27	48.33	45.33	51.67	64.45	68.00	55.56	56.41
Human + search	81.33	85.56	68.00	74.17	86.67	78.03	78.89	74.00	74.17	84.44	86.67	79.63	78.83
70B-Scale MLLMs													
InternVL2-76B [6]	62.50	74.04	60.00	41.04	76.43	59.22	78.40	51.11	56.25	43.82	55.42	57.90	58.68
Qwen2-VL-72B [36]	63.16	75.96	59.31	40.24	77.14	59.34	80.80	42.96	59.82	65.17	66.27	62.32	60.55
Specialist Grounding Models													
YOLO-World [7]	41.45	28.85	8.28	14.74	30.71	23.36	50.40	2.22	24.11	1.12	3.61	17.83	21.11
G-DINO-1.6-Pro [34]	39.47	41.35	48.97	23.11	24.29	33.59	44.00	40.00	39.29	32.58	27.71	37.68	35.25
DINO-X [31]	43.42	49.04	42.76	28.29	41.43	38.89	62.40	35.56	48.21	31.46	49.40	45.77	41.69
7B-Scale MLLMs													
Shikra-7B [3]	20.39	25.96	15.17	16.33	28.57	20.33	51.20	19.26	25.00	16.85	22.89	27.94	23.43
CogVLM-G [37]	46.71	64.42	49.66	34.26	63.57	48.61	79.20	31.11	54.46	56.18	66.27	56.43	51.80
DeepSeek-VL2 [40]	51.32	60.57	53.10	29.08	63.57	47.98	62.40	35.56	50.89	44.94	39.76	47.06	47.60
InternVL2-8B [6]	46.05	52.88	40.69	26.29	50.71	40.53	64.80	34.81	45.54	41.57	25.30	43.57	41.77
Qwen2-VL-7B [36]	48.03	74.04	51.30	33.07	65.71	50.38	76.00	33.33	54.46	57.30	59.04	55.33	52.40
Qwen2-VL-7B (SFT)	53.95	79.81	53.10	31.87	67.86	52.65	84.80	34.81	54.46	40.45	53.01	56.25	54.12
DeepPerception	69.08	86.54	64.14	41.04	77.86	63.13	85.60	40.74	58.04	59.55	61.45	60.85	62.20

Table 1. KVG results of DeepPerception and baseline models.

Models	Dog	Bird	Air.	Flwr.	Pet	Car	Avg.
LLaVA 1.5 [20]	38.96	35.24	34.71	51.37	52.25	46.92	43.24
Phi-3-Vision [1]	39.80	37.63	42.33	51.59	56.36	54.50	47.04
Idefics2 [18]	57.96	47.17	56.23	72.78	81.28	80.25	65.95
Finedefics [11]	72.86	57.61	63.82	89.88	92.18	84.67	76.84
Qwen2VL-7B [36]	71.39	65.31	71.77	86.78	91.25	90.95	79.57
DeepPerception	78.29	67.86	75.31	93.06	93.00	91.75	83.21

Table 2. FGVR results of DeepPerception and baseline models.

Models	MMBench-V1.1 _{test}	MMMU _{val}	AI2D	MathVision
Qwen2VL-7B ¹	82.0	50.0	79.4	18.6
DeepPerception	81.1	49.8	80.2	18.8

Table 3. Performance Comparison of DeepPerception and Qwen2VL-7B on general multimodal benchmarks.

rich knowledge. Several MLLMs with strong visual grounding capability were selected for comparison. For 70B-scale models, we used InternVL2-Llama3-76B [6] and Qwen2VL-72B [36]. For 7B-scale models, we used Shikra [3], CogVLM-Grounding [37], DeepSeek-VL-2 [40], InternVL2-8B [6], and Qwen2-VL-7B [36]. Additionally, we conducted comparisons with three specialist models: YOLO-World [7], GroundingDINO-1.6-Pro [34] and DINO-X [31].

Evaluation Settings. We evaluate all methods both on KVG-Bench and the FGVR task. For KVG-Bench, we adopt accuracy as the evaluation metric as in traditional REC [3, 36, 45]. Specifically, given a predicted bounding

box \tilde{B} and ground-truth bounding box B , we compute their IoU and classify the prediction as correct if $\text{IoU} \geq 0.5$. For FGVR, we follow the exact test settings with Finedefics [11] to frame it as a multi-choice task. To calculate the average accuracy across multiple categories, we compute a weighted average based on the number of instances per category.

Training Details. We adopt 8 NVIDIA A100 GPUs with 80G of memory. All seeds are fixed during the training procedures. We use Adam optimizer [15] with learning rate as $5e-6$, $\beta_1 = 0.9$, $\beta_2 = 0.999$, and $\varepsilon = 1e-8$ in the CoT-SFT stage and AdamW optimizer [22] with learning rate as $1e-6$, $\beta_1 = 0.9$, $\beta_2 = 0.999$, and $\varepsilon = 1e-6$ in the GRPO stage. The accumulated batch size is set to 16 in both stages. The GRPO stage employs a maximum completion length of 512 tokens with 4 samples per input.

5.2. Main Results

As demonstrated in Tab. 1, our DeepPerception model achieves significant performance improvements by integrating cognitive visual perception capabilities, validating the hypothesis that human-inspired cognition-perception synergy enhances visual perception. On in-domain categories, the model attains 63.13% average accuracy, surpassing all 7B-scale baselines (e.g., +10.5% over SFT) and outperforming 70B-scale models such as InternVL2-Llama3-76B (59.22%). For out-of-domain generalization, it achieves 60.85% accuracy—comparable to 70B-scale

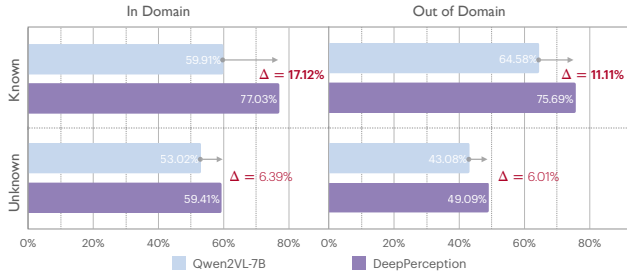


Figure 4. Knowledge evaluation results. DeepPerception exhibits greater improvement on known entities across domains, evidencing cognitive visual perception with structured knowledge integration rather than superficial perceptual improvements.

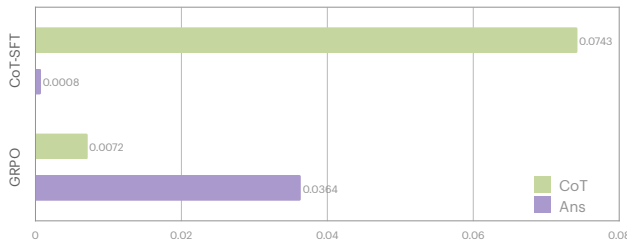


Figure 5. KL Divergence analysis between the probability distribution of response tokens from stage-2 models and the stage-1 model reveals complementary specialization: CoT-SFT focuses on knowledge-guided reasoning process (higher CoT divergence) while GRPO optimizes perceptual precision (elevated answer divergence), synergistically bridging cognitive processing and perception refinement.

models—while demonstrating near-human performance in categories where the model possesses richer knowledge, such as Dog (85.60% vs. human evaluators’ 78.89%).

These results confirm that DeepPerception’s success stems from its ability to emulate human-like cognitive processes: iterative knowledge-guided reasoning refines perceptual hypotheses (e.g., verifying anatomical features step-wise), while reinforcement learning aligns these hypotheses with precise visual outputs. The consistent superiority over non-cognitive baselines, particularly in fine-grained categories like Car (86.54% vs. human 85.56%), proves that structured knowledge integration—not mere visual memorization—drives performance gains. By bridging knowledge reasoning with perception, DeepPerception establishes new state-of-the-art results on KVG-Bench, demonstrating that cognitive mechanisms central to biological vision can be effectively operationalized in multimodal AI systems.

FGVR. To validate the generalizability of cognitive visual perception, we conducted experiments on FGVR datasets. Unlike the two-stage training paradigm used for KVG, only the reinforcement learning phase was applied here, as base models already exhibit strong baseline performance on FGVR. As shown in Tab. 2, our Deep-

Stage	Method	In Domain	Out of Domain	Overall
1	SFT	52.65	56.25	54.12
	CoT-SFT	56.82	56.80	56.81
2	CoT-SFT	56.94	56.99	56.96
	GRPO	63.13	60.85	62.20

Table 4. Ablation study on the effectiveness of the proposed two-stage cognitive training framework.

Perception model achieves state-of-the-art results across all categories, demonstrating universal performance gains: DeepPerception achieves state-of-the-art results across all FGVR categories (83.21% average accuracy), outperforming Qwen2-VL-7B by +3.64%. This evidence strongly supports that cognitive visual perception, characterized by iterative knowledge-visual alignment, provides universal benefits for fine-grained perception, mirroring human experts’ ability to combine sensory input with conceptual understanding.

General Capability. To comprehensively assess the model’s general capabilities across diverse multimodal scenarios, we conducted evaluations on established multimodal benchmarks. As shown in Tab. 3, DeepPerception maintains performance comparable to the base model, demonstrating preserved general capabilities without degradation.

5.3. Ablation Study

As shown in Tab. 4, our ablation study systematically evaluates the contributions of the two-stage training:

Stage-1. Replacing standard SFT with CoT-SFT elevates performance on seen categories from 52.65% to 56.82% while sustaining strong generalization on unseen categories (56.25%→56.80%), demonstrating that cognitive process integration enhances perceptual capabilities beyond conventional training.

Stage-2. The GRPO method achieves significant gains over CoT-SFT in stage-2, with in-domain accuracy rising to 63.13% (+6.19%) and out-of-domain accuracy reaching 60.85% (+3.86%). Combined with the KL Divergence analysis (Fig. 5), this confirms GRPO’s unique capability to translate refined reasoning into precise perceptual outputs (bounding box coordinates).

The results reveal that structured cognition enhancement and perception refinement are complementary and critical for resolving fine-grained ambiguities. This validates our hypothesis that mimicking human-like cognition-perception interaction is essential for advancing visual perception of MLLMs.

5.4. Analysis

To gain deeper insights into our model’s capabilities, we conducted the following analysis of its cognitive visual perception mechanisms:

How knowledge influences perception. We systematically evaluated the base model’s knowledge by probing entity-specific discriminative features and validating factual alignment against Wikipedia references using Qwen2.5-14B [42]. Entities were then classified into four groups based on knowledge possession (Known/Unknown) and training data presence (in-domain/out-of-domain). As evidenced in Fig. 4, DeepPerception achieves significantly greater performance gains on known entities versus unknown entities regardless of domain boundaries, confirming that its improvements originate from knowledge-driven cognitive processing rather than superficial perceptual enhancements, thereby validating its capacity to *harness domain knowledge for visual perception*. This aligns with human experts’ reliance on domain expertise to resolve ambiguity, confirming our framework’s success in emulating cognitive visual perception.

The roles of CoT-SFT and GRPO. As shown in Fig. 5, we quantified the impact of our two-stage training paradigm by measuring the KL Divergence between stage-2 models (trained with CoT-SFT or GRPO) and the stage-1 model, separately evaluating the CoT and answer components. For CoT-SFT, the significantly higher KL Divergence in the CoT components versus answer segments indicates that *CoT-SFT primarily equips the model with perception-oriented reasoning capabilities*. In contrast, GRPO exhibited greater divergence in the answer components than in the CoT, demonstrating its focus on *refining perceptual accuracy* grounded in the reasoning process. By combining the two stages, the framework achieves synergistic enhancement of cognitive visual perception, effectively bridging knowledge-driven reasoning and sensory processing.

Qualitative Results. As illustrated in Fig. 6, we conducted a comparative case analysis between DeepPerception and Qwen2-VL-7B. The visual evidence demonstrates our model’s capability to generate accurate answers through a reasoning process that systematically integrates domain-specific knowledge with visual observations, in contrast to the baseline model’s tendency to produce incorrect responses from superficial pattern recognition.

5.5. Discussion

We discuss two empirical findings of GRPO, with detailed results provided in the appendix: (1) Unlike DeepSeek-R1-Zero’s [10] progressive increase in response length during training, GRPO training on both KVG and FGVR data exhibits stable completion lengths fluctuating within specific ranges, suggesting bounded reasoning complexity in visual perception tasks; (2) We observed instances where incorrect cot rationales led to correct answers, indicating that the presence of cognitive processes, rather than their length or even factual accuracy, is the primary determinant of performance improvement. Detailed results are provided in

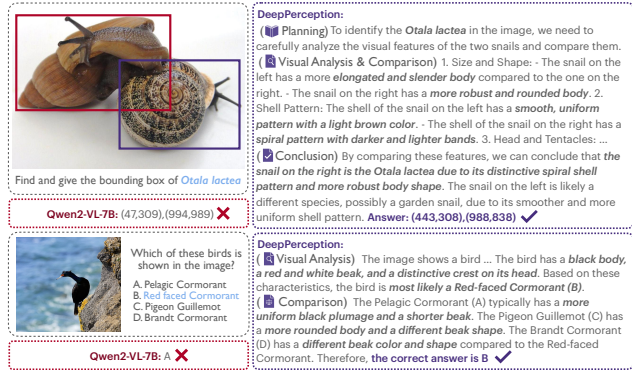


Figure 6. Case study comparing DeepPerception and Qwen2-VL-7B on KVG-Bench (top) and FGVR (bottom).

Appendix C.4.

6. Conclusion

In summary, this work demonstrates that embedding cognitive visual perception—characterized by perception enhancement through the integration of knowledge and reasoning—significantly enhances fine-grained visual perception in MLLMs. Our DeepPerception model achieves state-of-the-art performance on both KVG and FGVR tasks, outperforming 7B-scale baselines and rivaling 70B-scale models. Extensive experiments and analyses reveal that the two-stage training paradigm enables the model to effectively leverage cognitive mechanisms to refine perception, as evidenced by consistent improvements across domains. These findings establish cognitive enhancement as a pivotal direction for advancing fine-grained perception and comprehension in MLLMs.

References

- [1] Marah Abdin, Jyoti Aneja, Hany Awadalla, Ahmed Awadallah, Ammar Ahmad Awan, Nguyen Bach, Amit Bahree, Arash Bakhtiari, Jianmin Bao, Harkirat Behl, et al. Phi-3 technical report: A highly capable language model locally on your phone. *arXiv preprint arXiv:2404.14219*, 2024. 6
- [2] Lukas Bossard, Matthieu Guillaumin, and Luc Van Gool. Food-101—mining discriminative components with random forests. In *Computer vision—ECCV 2014: 13th European conference, zurich, Switzerland, September 6–12, 2014, proceedings, part VI 13*, pages 446–461. Springer, 2014. 5, 10
- [3] Keqin Chen, Zhao Zhang, Weili Zeng, Richong Zhang, Feng Zhu, and Rui Zhao. Shikra: Unleashing multimodal llm’s referential dialogue magic. *arXiv preprint arXiv:2306.15195*, 2023. 2, 6, 12
- [4] Zhenfang Chen, Peng Wang, Lin Ma, Kwan-Yee K Wong, and Qi Wu. Cops-ref: A new dataset and task on compositional referring expression comprehension. In *Proceedings of the IEEE/CVF Conference on Computer Vision and Pattern Recognition*, pages 10086–10095, 2020. 3

- [5] Zhihong Chen, Ruifei Zhang, Yibing Song, Xiang Wan, and Guanbin Li. Advancing visual grounding with scene knowledge: Benchmark and method. In *Proceedings of the IEEE/CVF Conference on Computer Vision and Pattern Recognition*, pages 15039–15049, 2023. 3
- [6] Zhe Chen, Weiyun Wang, Yue Cao, Yangzhou Liu, Zhangwei Gao, Erfei Cui, Jinguo Zhu, Shenglong Ye, Hao Tian, Zhaoyang Liu, et al. Expanding performance boundaries of open-source multimodal models with model, data, and test-time scaling. *arXiv preprint arXiv:2412.05271*, 2024. 2, 6
- [7] Tianheng Cheng, Lin Song, Yixiao Ge, Wenyu Liu, Xinggang Wang, and Ying Shan. Yolo-world: Real-time open-vocabulary object detection. In *Proc. IEEE Conf. Computer Vision and Pattern Recognition (CVPR)*, 2024. 6, 12
- [8] Linger Deng, Yuliang Liu, Bohan Li, Dongliang Luo, Liang Wu, Chengquan Zhang, Pengyuan Lyu, Ziyang Zhang, Gang Zhang, Errui Ding, et al. R-cot: Reverse chain-of-thought problem generation for geometric reasoning in large multimodal models. *arXiv preprint arXiv:2410.17885*, 2024. 2
- [9] E Bruce Goldstein. *Cognitive psychology: Connecting mind, research and everyday experience*. Wadsworth Publishing, 2007. 2
- [10] Daya Guo, Dejian Yang, Haowei Zhang, Junxiao Song, Ruoyu Zhang, Runxin Xu, Qihao Zhu, Shirong Ma, Peiyi Wang, Xiao Bi, et al. Deepseek-r1: Incentivizing reasoning capability in llms via reinforcement learning. *arXiv preprint arXiv:2501.12948*, 2025. 4, 5, 8, 13
- [11] Hulingxiao He, Geng Li, Zijun Geng, Jinglin Xu, and Yuxin Peng. Analyzing and boosting the power of fine-grained visual recognition for multi-modal large language models. In *The Thirteenth International Conference on Learning Representations*, 2025. 6
- [12] Jay Hegd . Time course of visual perception: coarse-to-fine processing and beyond. *Progress in neurobiology*, 84(4):405–439, 2008. 2
- [13] Sahar Kazemzadeh, Vicente Ordonez, Mark Matten, and Tamara Berg. Referitgame: Referring to objects in photographs of natural scenes. In *Proceedings of the 2014 conference on empirical methods in natural language processing (EMNLP)*, pages 787–798, 2014. 2, 3
- [14] Aditya Khosla, Nityananda Jayadevaprakash, Bangpeng Yao, and Li Fei-Fei. Novel dataset for fine-grained image categorization. In *First Workshop on Fine-Grained Visual Categorization, IEEE Conference on Computer Vision and Pattern Recognition*, Colorado Springs, CO, 2011. 3, 5, 10
- [15] Diederik P. Kingma and Jimmy Ba. Adam: A method for stochastic optimization. In *3rd International Conference on Learning Representations, ICLR 2015, San Diego, CA, USA, May 7-9, 2015, Conference Track Proceedings*, 2015. 6, 12
- [16] Jonathan Krause, Michael Stark, Jia Deng, and Li Fei-Fei. 3d object representations for fine-grained categorization. In *Proceedings of the IEEE international conference on computer vision workshops*, pages 554–561, 2013. 3, 5, 10
- [17] Xin Lai, Zhuotao Tian, Yukang Chen, Yanwei Li, Yuhui Yuan, Shu Liu, and Jiaya Jia. Lisa: Reasoning segmentation via large language model. In *Proceedings of the IEEE/CVF Conference on Computer Vision and Pattern Recognition*, pages 9579–9589, 2024. 2, 3
- [18] Hugo Lauren¸on, L o Tronchon, Matthieu Cord, and Victor Sanh. What matters when building vision-language models? *Advances in Neural Information Processing Systems*, 37:87874–87907, 2025. 6
- [19] Haotian Liu, Chunyuan Li, Qingyang Wu, and Yong Jae Lee. Visual instruction tuning. *Advances in neural information processing systems*, 36:34892–34916, 2023. 2
- [20] Haotian Liu, Chunyuan Li, Yuheng Li, and Yong Jae Lee. Improved baselines with visual instruction tuning. In *Proceedings of the IEEE/CVF Conference on Computer Vision and Pattern Recognition (CVPR)*, pages 26296–26306, 2024. 2, 6
- [21] Runtao Liu, Chenxi Liu, Yutong Bai, and Alan L Yuille. Clevr-ref+: Diagnosing visual reasoning with referring expressions. In *Proceedings of the IEEE/CVF conference on computer vision and pattern recognition*, pages 4185–4194, 2019. 3
- [22] Ilya Loshchilov and Frank Hutter. Decoupled weight decay regularization. In *International Conference on Learning Representations*, 2019. 6, 12
- [23] Chuofan Ma, Yi Jiang, Jiannan Wu, Zehuan Yuan, and Xiaojuan Qi. Groma: Localized visual tokenization for grounding multimodal large language models. In *European Conference on Computer Vision*, pages 417–435. Springer, 2024. 2
- [24] Subhransu Maji, Esa Rahtu, Juho Kannala, Matthew Blaschko, and Andrea Vedaldi. Fine-grained visual classification of aircraft. *arXiv preprint arXiv:1306.5151*, 2013. 3, 5, 10, 11
- [25] Junhua Mao, Jonathan Huang, Alexander Toshev, Oana Camburu, Alan L Yuille, and Kevin Murphy. Generation and comprehension of unambiguous object descriptions. In *Proceedings of the IEEE conference on computer vision and pattern recognition*, pages 11–20, 2016. 3
- [26] Maria-Elena Nilsback and Andrew Zisserman. Automated flower classification over a large number of classes. In *2008 Sixth Indian conference on computer vision, graphics & image processing*, pages 722–729. IEEE, 2008. 3, 5, 10
- [27] OpenAI. GPT4 technical report. *arXiv preprint arXiv:2303.08774*, 2023. 10
- [28] OpenAI. Hello gpt-4, 2024. 2
- [29] Zhiliang Peng, Wenhui Wang, Li Dong, Yaru Hao, Shaohan Huang, Shuming Ma, and Furu Wei. Kosmos-2: Grounding multimodal large language models to the world. *arXiv preprint arXiv:2306.14824*, 2023. 2
- [30] Yanyuan Qiao, Chaorui Deng, and Qi Wu. Referring expression comprehension: A survey of methods and datasets. *IEEE Transactions on Multimedia*, 23:4426–4440, 2020. 3
- [31] Tianhe Ren, Yihao Chen, Qing Jiang, Zhaoyang Zeng, Yuda Xiong, Wenlong Liu, Zhengyu Ma, Junyi Shen, Yuan Gao, Xiaoke Jiang, Xingyu Chen, Zhuheng Song, Yuhong Zhang, Hongjie Huang, Han Gao, Shilong Liu, Hao Zhang, Feng Li, Kent Yu, and Lei Zhang. Dino-x: A unified vision model for open-world object detection and understanding, 2024. 6, 12
- [32] Wenhao Shi, Zhiqiang Hu, Yi Bin, Junhua Liu, Yang Yang, See-Kiong Ng, Lidong Bing, and Roy Ka-Wei Lee. Math-LLaVA: Bootstrapping mathematical reasoning for multimodal large language models. In *Findings of the Association*

- for *Computational Linguistics: EMNLP 2024*, pages 4663–4680, Miami, Florida, USA, 2024. Association for Computational Linguistics. 2, 3
- [33] James W Tanaka and Marjorie Taylor. Object categories and expertise: Is the basic level in the eye of the beholder? *Cognitive psychology*, 23(3):457–482, 1991. 2
- [34] Ren Tianhe, Huang Hongjie, and Jiang Xiaoke. Grounding dino 1.6, 2024. 6, 12
- [35] Grant Van Horn, Oisín Mac Aodha, Yang Song, Yin Cui, Chen Sun, Alex Shepard, Hartwig Adam, Pietro Perona, and Serge Belongie. The inaturalist species classification and detection dataset. In *Proceedings of the IEEE conference on computer vision and pattern recognition*, pages 8769–8778, 2018. 5, 10, 11
- [36] Peng Wang, Shuai Bai, Sinan Tan, Shijie Wang, Zhihao Fan, Jinze Bai, Keqin Chen, Xuejing Liu, Jialin Wang, Wenbin Ge, et al. Qwen2-vl: Enhancing vision-language model’s perception of the world at any resolution. *arXiv preprint arXiv:2409.12191*, 2024. 2, 4, 5, 6, 11
- [37] Weihang Wang, Qingsong Lv, Wenmeng Yu, Wenyi Hong, Ji Qi, Yan Wang, Junhui Ji, Zhuoyi Yang, Lei Zhao, Song XiXuan, Jiazheng Xu, Keqin Chen, Bin Xu, Juanzi Li, Yuxiao Dong, Ming Ding, and Jie Tang. CogVLM: Visual expert for pretrained language models. In *The Thirty-eighth Annual Conference on Neural Information Processing Systems*, 2024. 6
- [38] Peter Welinder, Steve Branson, Takeshi Mita, Catherine Wah, Florian Schroff, Serge Belongie, and Pietro Perona. Caltech-ucsd birds 200. 2010. 3
- [39] T. Weyand, A. Araujo, B. Cao, and J. Sim. Google Landmarks Dataset v2 - A Large-Scale Benchmark for Instance-Level Recognition and Retrieval. In *Proc. CVPR*, 2020. 5, 10
- [40] Zhiyu Wu, Xiaokang Chen, Zizheng Pan, Xingchao Liu, Wen Liu, Damai Dai, Huazuo Gao, Yiyang Ma, Chengyue Wu, Bingxuan Wang, et al. Deepseek-vl2: Mixture-of-experts vision-language models for advanced multimodal understanding. *arXiv preprint arXiv:2412.10302*, 2024. 6, 12
- [41] Guowei Xu, Peng Jin, Li Hao, Yibing Song, Lichao Sun, and Li Yuan. Llava-o1: Let vision language models reason step-by-step. *arXiv preprint arXiv:2411.10440*, 2024. 2, 3
- [42] An Yang, Baosong Yang, Beichen Zhang, Binyuan Hui, Bo Zheng, Bowen Yu, Chengyuan Li, Dayiheng Liu, Fei Huang, Haoran Wei, Huan Lin, Jian Yang, Jianhong Tu, Jianwei Zhang, Jianxin Yang, Jiayi Yang, Jingren Zhou, Junyang Lin, Kai Dang, Keming Lu, Keqin Bao, Kexin Yang, Le Yu, Mei Li, Mingfeng Xue, Pei Zhang, Qin Zhu, Rui Men, Runji Lin, Tianhao Li, Tingyu Xia, Xingzhang Ren, Xuancheng Ren, Yang Fan, Yang Su, Yichang Zhang, Yu Wan, Yuqiong Liu, Zeyu Cui, Zhenru Zhang, and Zihan Qiu. Qwen2.5 technical report. *arXiv preprint arXiv:2412.15115*, 2024. 8, 12
- [43] Huanjin Yao, Jiaying Huang, Wenhao Wu, Jingyi Zhang, Yibo Wang, Shunyu Liu, Yingjie Wang, Yuxin Song, Haocheng Feng, Li Shen, et al. Mulberry: Empowering mllm with o1-like reasoning and reflection via collective monte carlo tree search. *arXiv preprint arXiv:2412.18319*, 2024. 2
- [44] Yuan Yao, Tianyu Yu, Ao Zhang, Chongyi Wang, Junbo Cui, Hongji Zhu, Tianchi Cai, Haoyu Li, Weilin Zhao, Zhihui He, et al. Minicpm-v: A gpt-4v level mllm on your phone. *arXiv preprint arXiv:2408.01800*, 2024. 2
- [45] Haoxuan You, Haotian Zhang, Zhe Gan, Xianzhi Du, Bowen Zhang, Zirui Wang, Liangliang Cao, Shih-Fu Chang, and Yinfei Yang. Ferret: Refer and ground anything anywhere at any granularity. In *The Twelfth International Conference on Learning Representations*, 2024. 2, 6
- [46] Licheng Yu, Patrick Poirson, Shan Yang, Alexander C Berg, and Tamara L Berg. Modeling context in referring expressions. In *Computer Vision—ECCV 2016: 14th European Conference, Amsterdam, The Netherlands, October 11–14, 2016, Proceedings, Part II 14*, pages 69–85. Springer, 2016. 2, 3
- [47] Xiang Yue, Yuansheng Ni, Kai Zhang, Tianyu Zheng, Ruoqi Liu, Ge Zhang, Samuel Stevens, Dongfu Jiang, Weiming Ren, Yuxuan Sun, et al. Mmmu: A massive multi-discipline multimodal understanding and reasoning benchmark for expert agi. In *Proceedings of the IEEE/CVF Conference on Computer Vision and Pattern Recognition*, pages 9556–9567, 2024. 2
- [48] Renrui Zhang, Dongzhi Jiang, Yichi Zhang, Haokun Lin, Ziyu Guo, Pengshuo Qiu, Aojun Zhou, Pan Lu, Kai-Wei Chang, Yu Qiao, et al. Mathverse: Does your multi-modal llm truly see the diagrams in visual math problems? In *European Conference on Computer Vision*, pages 169–186, 2024. 2

A. KVG-Bench

This section details the data collection and annotation protocol for KVG-Bench.

A.1. Data Collection

Category Selection Ten categories were strategically curated from established fine-grained visual recognition (FVGR) datasets including FGVC-Aircraft [24], Stanford-Cars [16], iNaturalist2017 [35], Food101 [2], Stanford-Dogs [14], Flower-102 [26], and Google-Landmarks-v2 [39]. Categories requiring ambiguous spatial localization (e.g., ”sports” and ”scenes”) were systematically excluded.

Entity List Curation We built the list of detailed entity names through a step-by-step process. First, we started with existing names from aforementioned FVGR datasets to make sure they fit the right categories. Then, we used ChatGPT [27] to collect more entities in these categories by querying with category name and example entities. Finally, we checked all these entity names against Wikipedia to confirm their accuracy and avoid confusing or incorrect terms.

Web Image Retrieval The image collection process employed diversified search strategies, systematically generating query variations (e.g., “X versus Y”, “X compared to Y”, “differences between X and Y”) to retrieve visually discriminative instances across search engines. The image collection process focused on two core principles: diversity and challenge. To ensure diversity, images were collected to encompass a variety of distinct entities within each category, achieved through systematically varied search query combinations. This approach guaranteed a wide range of entity interactions and visual scenarios. For challenge, we specifically selected images containing multiple entities from the same category (requires fine-grained visual discrimination) or exhibited high visual similarity with subtle distinguishing features.

A.2. Annotation

The annotation process prioritized quality control. Five annotators manually annotated each image with bounding boxes and entity labels by cross-referencing contextual information (e.g. caption, webpage metadata) with authoritative sources (e.g., Wikipedia entries) to verify entity identities. To ensure consistency, the annotations underwent independent re-evaluation by annotators who did not participate in the initial labeling, with conflicting cases cross-verified through multi-annotator reconciliation and persistently inconsistent instances eliminated to ensure annotation accuracy.

B. Method

This section elaborates on the implementation details of the proposed method.

B.1. Data Engine

Our data processing pipeline comprises three core stages: categorization, fine-grained annotation, and image composition.

Categorization. We first categorize the data based on dataset sources. For example, data from FGVC-Aircraft [24] is directly classified as aircraft. Second, for datasets covering multiple categories such as iNaturalist2017 [35], we subdivide entities into finer-grained categories (e.g., mammal, bird, etc.) based on their annotations. Finally, the data is divided into ten distinct categories: aircraft, car, reptilia, bird, food, dog, mollusca, mammal, flower, and landmark. The data from the first five categories are used for training, while the data from the last five categories are solely used to construct the entity list for testing purposes.

Fine-grained Annotation. To acquire bounding box annotation, we employed the Qwen2-VL-7B [36] model for

visual grounding. Given that each image already possessed verified ground truth labels where the corresponding entities were guaranteed to be present, we directly utilized these textual labels as prompts to generate precise bounding box annotations through the model’s visual-language alignment capabilities. Given an image and its entity label E , we input the structured query: “Find and give the bounding box of $\{E\}$ ” to generate bounding box coordinates. After the automatic annotation, we randomly sample the annotated data for manual verification. The results show that the accuracy of the automatic annotations exceeds 95%, allowing us to consider the resulting bounding boxes as approximations of the ground truth.

Image Composition. For each category-specific dataset \mathcal{D}_c , we implement an iterative sampling protocol without replacement, where the sample size k is stochastically determined as $k \sim P_{sel}(2 \leq k \leq 6)$ per iteration, where P_{sel} is a pre-defined discrete distribution over range $[2, 6]$. This process strictly enforces entity exclusivity by guaranteeing $\bigcap_{i=1}^k E_i = \emptyset$ across all sampled instances, where E_i denotes the entity in the i -th sample. The sampled images are then composited using four layout strategies: horizontal tiling, vertical stacking, grid arrangement, and random placement. For each sampled batch, we randomly select one composition method and apply corresponding geometric transformations to adjust the original bounding box coordinates to their correct positions in the synthesized images. This spatial adaptation process preserves annotation consistency while creating multi-instance scenes. The final augmented dataset \mathcal{D}'_c contains composite images with transformed bounding boxes and preserved entity labels, where each composite image integrates multiple object instances from the original samples. The dataset is then partitioned into two disjoint subsets for subsequent two-stage training.

B.2. Chain-of-Thought Data Generation

We employ Qwen2-VL-72B [36] to generate Chain-of-Thought (CoT) rationales. Specifically, the model takes the image, ground-truth entity annotations (names and bounding boxes), and a CoT generation instruction as input, producing detailed reasoning processes for training. Fig. 7 illustrates a representative training instance.

C. Experiment

This section provides additional details about the experiments and analysis, along with discussions on empirical findings.

C.1. Implementation Details

Baseline Models. When evaluating certain baseline models, some adjustments were made to accommodate minor

CoT Generation Prompt

`;`—vision_start—`;`Image.jpg`;`—vision_end—`;`

This image shows [entity₁] ([bbox₁]), [entity₂] ([bbox₂]), . . . , and [entity_n] ([bbox_n]).

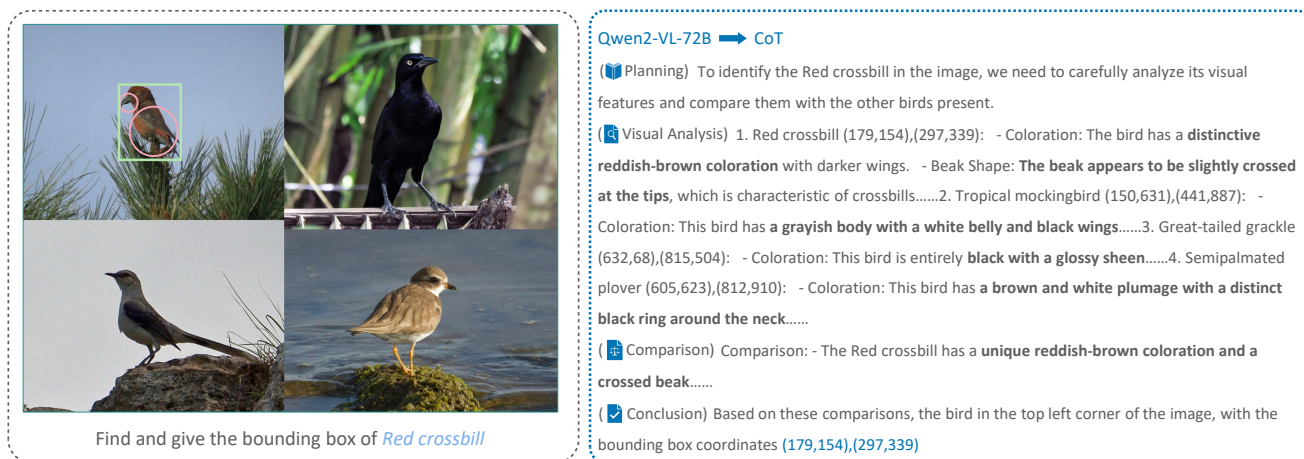
The bounding box of [target entity] is [target bbox].

Give the reasoning process that would identify it based on the image and your knowledge

Note that you **MUST** pay attention to the differences from other objects of the same type in this image and make a detailed comparison between them to find evidence that distinguishes this object from the others

Note that you **MUST** first analyze the visual features that help you make a judgment, and then compare the objects

Note that when an object is “[Unknown]”, you can still make a comparison based on its visual features without knowing its name



Qwen2-VL-72B → CoT

- 📌 Planning) To identify the Red crossbill in the image, we need to carefully analyze its visual features and compare them with the other birds present.
- 👁️ Visual Analysis) 1. Red crossbill (179,154),(297,339): - Coloration: The bird has a **distinctive reddish-brown coloration** with darker wings. - Beak Shape: **The beak appears to be slightly crossed at the tips**, which is characteristic of crossbills.....2. Tropical mockingbird (150,631),(441,887): - Coloration: This bird has a **grayish body with a white belly and black wings**.....3. Great-tailed grackle (632,68),(815,504): - Coloration: This bird is entirely **black with a glossy sheen**.....4. Semipalmated plover (605,623),(812,910): - Coloration: This bird has a **brown and white plumage with a distinct black ring around the neck**.....
- 🔍 Comparison) Comparison: - The Red crossbill has a **unique reddish-brown coloration and a crossed beak**.....
- ✅ Conclusion) Based on these comparisons, the bird in the top left corner of the image, with the bounding box coordinates (179,154),(297,339)

Find and give the bounding box of *Red crossbill*

Figure 7. Example of Chain-of-Thought data generated by Qwen2-VL-72B.

differences in their output formats. For DeepSeek-VL2 [40], the first output bounding box was selected as the model’s predicted answer for downstream evaluation. For the evaluation of GroundingDINO-1.6-Pro [34] and DINO-X [31], we used their official APIs (GroundingDINO API, DINO-X API) in `deepdataspace`. Images were converted to base64 format, with oversized images downsampled. Detection targets were fine-grained labels (e.g., “Buick Enclave”) instead of generic categories (e.g., “car”). API requests followed official configurations, and the highest-score bounding box was selected. YOLO-World [7] was evaluated locally under identical criteria. Regarding Shikra-7B [3], we have replicated the evaluation code based on the officially released model and code. However, the actual performance is significantly lower than that reported in the paper. Similar discrepancies have also been observed in replication attempts by other researchers.

Training Details. We use Adam optimizer [15] with learning rate as $5e - 6$, $\beta_1 = 0.9$, $\beta_2 = 0.999$, and $\epsilon = 1e - 8$ in the CoT-SFT stage and AdamW optimizer [22] with learning rate as $1e - 6$, $\beta_1 = 0.9$, $\beta_2 = 0.999$, and

$\epsilon = 1e - 6$ in the GRPO stage. The accumulated batch size is set to 16 in both stages. The GRPO stage employs a maximum completion length of 512 tokens with 4 samples per input.

C.2. Analysis

Knowledge Evaluation The knowledge evaluation operates through three sequential steps: (1) Knowledge Probing: For each entity in KVG-Bench, the model was prompted to generate discriminative visual features distinguishing it from same-category entities. (2) Reference Validation: Model outputs were evaluated against corresponding Wikipedia descriptions using Qwen2.5-14B [42] to measure factual consistency. (3) Entity Categorization: Entities were first categorized as Known (aligned with reference) or Unknown (divergent from reference), then further divided into four groups based on their presence in the training data.

KL Divergence Analysis Revised as Continuous Prose: To ensure equitable comparison of CoT-SFT and GRPO enhancements, we trained stage-1 models on identical data volumes using each method, followed by systematic evalua-

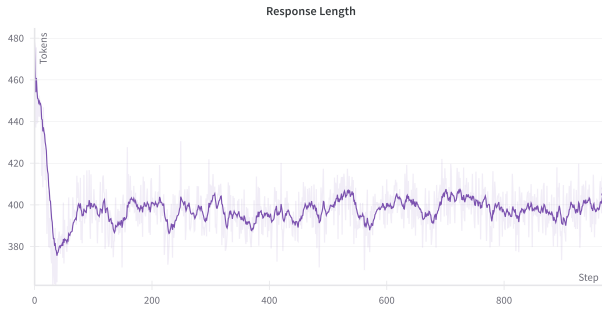


Figure 8. The average response length of DeepPerception on the KVG training data during the RL process

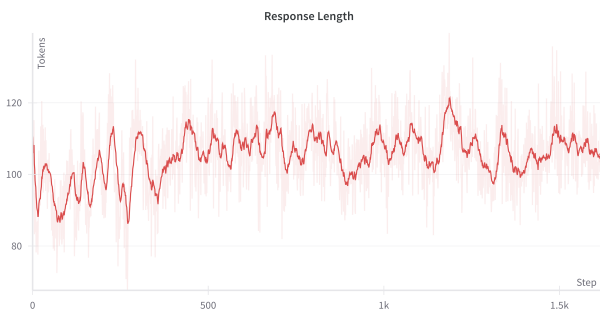


Figure 9. The average response length of DeepPerception on the FGVR training data during the RL process

tion of resultant stage-2 models on KVG-Bench. KL Divergence between stage-2 and stage-1 models was computed and split via the special token (“`;/think;`”) into CoT reasoning and answer components, with token-level averaging applied to both segments to mitigate the effect of length variation.

C.3. Qualitative Results

Figs. 10 and 11 present comparative analyses between DeepPerception and Qwen2-VL-7B on KVG-Bench and FGVR datasets, respectively. Extensive qualitative comparisons demonstrate DeepPerception’s substantial performance advantage in fine-grained visual perception tasks, attributable to its cognitive visual reasoning capabilities - a critical competency absent in Qwen2-VL-7B.

Fig. 12 illustrates atypical patterns including: (1) speculative reasoning (A/B hypotheses without definitive conclusions) and (2) reasoning-output discrepancies (divergent rationalization vs final answers). These cases suggest that *the presence of cognitive processes may hold greater significance than their factual accuracy* in cognitive visual perception.

C.4. Discussion

Our analysis of response length dynamics during GRPO training on KVG (Fig. 8) and FGVR (Fig. 9) datasets reveals stable length throughout optimization, diverging from the progressively increasing trends observed in DeepSeek-R1-Zero [10]. Notably, while an initial sharp decline occurred in training on KVG, which was primarily attributable to the 512 tokens completion limit imposing penalties on lengthy responses, length stabilization ultimately prevailed. This stability is attributed to constrained reasoning complexity requirements in our tasks: unlike DeepSeek-R1-Zero’s multi-faceted reasoning paradigms, our framework operates through streamlined cognitive pathways that inherently limit verbose rationalization needs. The mechanisms underlying cognitive-perceptual alignment, particularly how flawed reasoning enables accurate perception, present a compelling avenue for future exploration into cognitive visual perception.

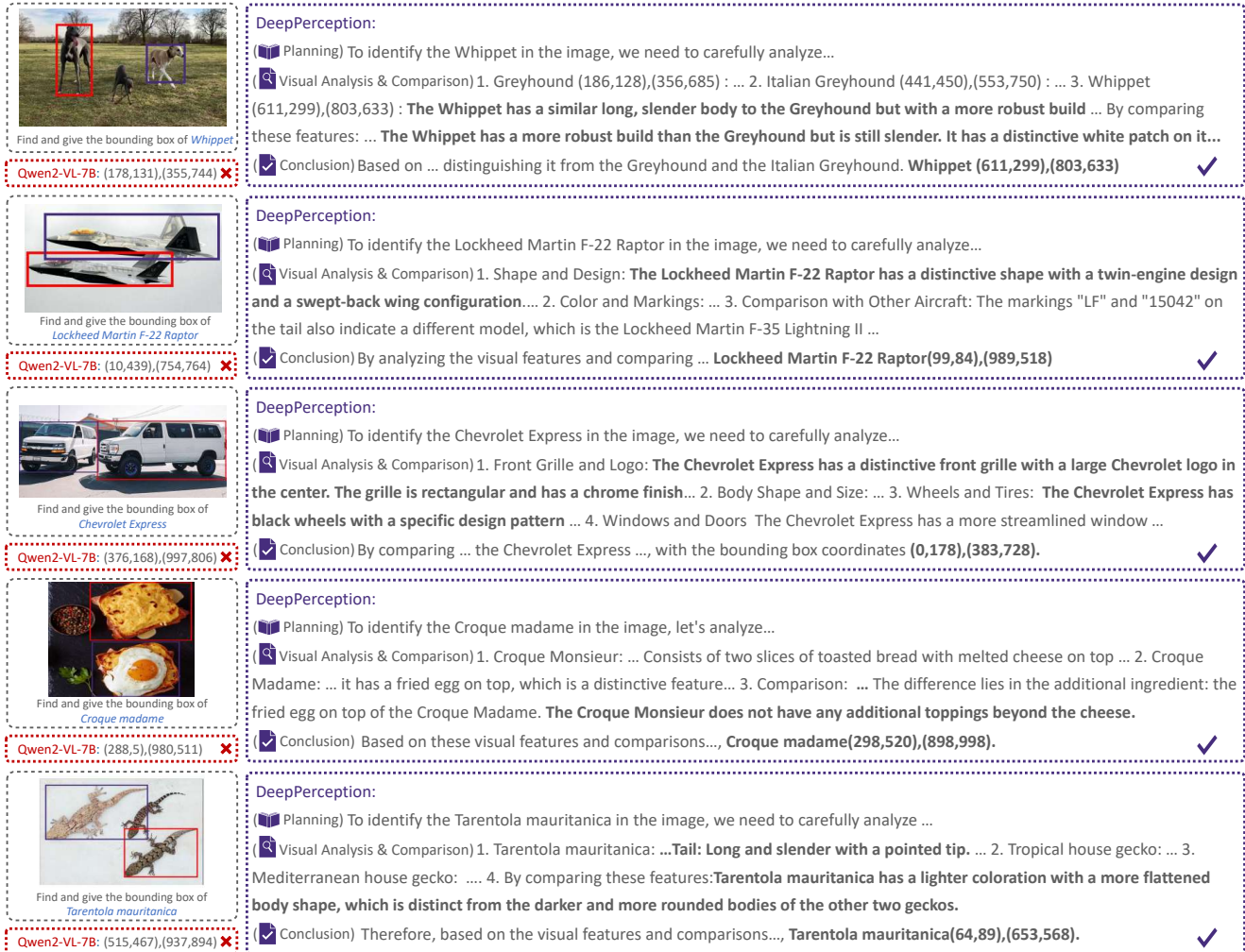


Figure 10. Case study comparing DeepPerception and Qwen2-VL-7B on KVG-Bench






 <p>Which of these aircrafts is shown in the image? A. 727-200 B. 707-320 C. MD-87 D. DC-9-30</p> <p>Qwen2-VL-7B: B ❌</p>	<p>DeepPerception:</p> <p>(Q Visual Analysis) The image shows an aircraft with a distinctive tail design and a fuselage that is longer than the typical 727-200.</p> <p>(C Comparison) The aircraft has a high-mounted horizontal stabilizer and a T-tail, which is characteristic of the Boeing 727. The fuselage length and the design of the engines suggest it is a 727-200.</p> <p>Therefore, the correct answer is : A. 727-200. ✓</p>
 <p>Which of these birds is shown in the image? A. Rusty Blackbird B. Bronzed Cowbird C. Shiny Cowbird D. Boat tailed Grackle</p> <p>Qwen2-VL-7B: C ❌</p>	<p>DeepPerception:</p> <p>(Q Visual Analysis) The bird in the image has a distinctive appearance with a brownish body and a black tail ...</p> <p>(C Comparison) The Rusty Blackbird is known for its brownish coloration and the Boat-tailed Grackle has a similar appearance. However, the Boat-tailed Grackle typically has a more prominent black tail and a different body shape. Based on the image, the bird appears to be more similar to the Rusty Blackbird in terms of coloration and body shape. Therefore, the correct answer is A. Rusty Blackbird. ✓</p>
 <p>Which of these cars is shown in the image? A. Audi TT Hatchback 2011 B. Audi TT RS Coupe 2012 C. Audi TTS Coupe 2012 D. Audi R8 Coupe 2012</p> <p>Qwen2-VL-7B: C ❌</p>	<p>DeepPerception:</p> <p>(Q Visual Analysis) The image shows a blue Audi car with a sporty design, including a rear spoiler and a distinctive grille. The car is a coupe, which rules out the hatchback option.</p> <p>(C Comparison) The Audi TT RS Coupe 2012 is known for its similar design features, including the rear spoiler and the overall shape of the car.</p> <p>Therefore, the correct answer is B. Audi TT RS Coupe 2012. ✓</p>
 <p>Which of these flowers is shown in the image? A. artichoke B. globe thistle C. spear thistle D. alpine sea holly</p> <p>Qwen2-VL-7B: B ❌</p>	<p>DeepPerception:</p> <p>(Q Visual Analysis) The image shows a flower with a central, spiky, greenish-brown core ... This matches the description of globe thistle (B. globe thistle) and alpine sea holly (D. alpine sea holly), both of which have similar characteristics.</p> <p>(C Comparison) However, globe thistle typically has more pronounced and dense flower heads, while alpine sea holly has a more open and airy appearance. The image does not show the dense, rounded flower head of globe thistle, but rather a more open and airy structure with long, narrow leaves. Therefore, the most likely answer is D. alpine sea holly. ✓</p>
 <p>Which of these pets is shown in the image? A. Ragdoll B. Birman C. Maine Coon D. Persian</p> <p>Qwen2-VL-7B: B ❌</p>	<p>DeepPerception:</p> <p>(Q Visual Analysis) The image shows a cat with a long, fluffy coat and a distinctive face with green eyes. The cat's fur is predominantly white with black and gray markings. Based on these characteristics, the cat appears to be a Maine Coon.</p> <p>(C Comparison) Ragdolls typically have a more relaxed and docile demeanor, Birman have a distinctive white coat with orange or cream-colored points, and Persians have a round face and a short, dense coat.</p> <p>Therefore, the correct answer is : C. Maine Coon ✓</p>

Figure 11. Case study comparing DeepPerception and Qwen2-VL-7B on FGVR



Which of these dogs is shown in the image?

- A. Japanese spaniel
- B. Pekinese
- C. Papillon
- D. Chihuahua

Qwen2-VL-7B: B



DeepPerception:

(🔍 Visual Analysis) The image shows a dog with a black and white coat, a small body, and a tail that is curled up.

(⚖️ Comparison) This matches the description of a Japanese Spaniel (A) and a Pekinese (B), both of which are small breeds with a similar appearance. The papillon (C) and Chihuahua (D) do not have the same coat pattern or body structure as the dog in the image. **Therefore, the correct answer is either A or B.**

Answer : A



Which of these birds is shown in the image?

- A. Laysan Albatross
- B. Sooty Albatross
- C. Pomarine Jaeger
- D. Black footed Albatross

Qwen2-VL-7B: C



DeepPerception:

(🔍 Visual Analysis) The image shows a bird with ...

(⚖️ Comparison) The bird's dark plumage and the context of the image suggest it is a Black-footed Albatross (D). Laysan Albatrosses (A) and Sooty Albatrosses (B) typically have a more white or grey plumage, respectively, while Pomarine Jaegers (C) are smaller and have a different body shape. **Therefore, the correct answer is D.**

Answer : B

Figure 12. Illustrative Cases of atypical CoT Reasoning